Suppression of Cross-Band Scattering in Interleaved Dual-Band Cellular Base-Station Antenna Arrays

HAI-HAN SUN [1,2], (Member, IEEE), BEVAN JONES[1], Y. JAY GUO[1], (Fellow, IEEE), AND YEE HUI LEE[2], (Senior Member, IEEE)

[1] Global Big Data Technologies Centre, Faculty of Engineering and Information Technology, University of Technology Sydney, Sydney, NSW 2007, Australia
[2] School of Electrical and Electronic Engineering, Nanyang Technological University, Singapore 639798

Corresponding author: Hai-Han Sun (haihan.sun199403@gmail.com)

ABSTRACT In this article, novel techniques to suppress cross-band scattering in interleaved dual-band base station antenna arrays are presented. Firstly, the detrimental effect of high-band (HB) elements on low-band (LB) radiation performance is theoretically analyzed. With a thorough analysis, a capacitance-loaded HB element is innovated to solve the issue and restore the LB patterns. Secondly, to eliminate the reverse HB scattering caused by the LB element while enhancing the bandwidth of the LB element, a novel double-arm choked cross-dipole configuration is proposed. A compact array section is built with these innovated elements. The experimental results of the array show a largely suppressed cross-band scattering with stable radiation performance across the well-matched bands, demonstrating the effectiveness of the presented techniques.

INDEX TERMS Bandwidth enhancement, base station antennas, common-mode resonance, cross-band scattering suppression, dual-band array.

I. INTRODUCTION

Dual-band antenna arrays with interleaved columns of low-band (LB) and high-band (HB) elements are widely used in modern cellular networks. They serve as an effective solution to simultaneously support different services while eliminating the need for new antenna sites and reducing the total cost of deployment. However, such dual-band arrays have an inherent problem of cross-band scattering. The scattering can become a very difficult problem when array columns in different bands are placed close to each other which is often the case. This frequently results in a significant degradation in antenna radiation performance.

The HB scattering caused by the LB element has been discussed in [1]. The physically large LB element behaves as a strong scatterer in the high band and has significant HB currents induced on it. These currents re-radiate and cause distortion of HB radiation patterns. Several solutions have been proposed to minimize the scattering and restore the HB patterns, including adding metal baffles or walls [2]–[4], using a stacked array configuration with HB elements mounted above LB elements [5]–[7], and using choking techniques [1].

The associate editor coordinating the review of this manuscript and approving it for publication was Davide Comite.

To be specific, metal baffles and walls separating the elements are commonly used in the embedded array configuration where HB elements are nested within LB elements [2]–[4]. The HB radiation patterns can be largely restored with the symmetrical array arrangement and with the help of the baffles and walls. However, there appears to be no systematic way of arriving at suitable arrangements and dimensions of the baffles. A stacked array configuration where HB elements are located above LB elements has been utilized in [5]–[7] to avoid the HB scattering from the LB element. In [5], the patch antennas operating in both bands are stacked with shaped reflectors and directors to improve the patterns. Symmetrical radiation patterns with high port isolations are achieved. In [6] and [7], a LB-pass HB-reflect surface is inserted between the LB and HB elements to reduce the profile of the stacked array. The surface acts as a capacitive loading for the LB antenna allowing its height to be reduced, and also acts as a ground plane for the HB elements. Such arrays have wide bandwidths and stable radiation performance at both bands with a low-profile structure. However, as mentioned in [7], this configuration is more suitable for dual-band array with large frequency ratios. The choking techniques presented in [1] minimize the scattering from the LB element by inserting chokes with HB-stop LB-pass property into the LB arms. The chokes effectively suppress

the HB induced currents on LB arms, making the LB element "invisible" in the high band so as to preserve the HB radiation performance. One limitation of this method is that the inserted chokes narrow the operating bandwidth of the LB element. The LB element presented in [1] only covers the 3G band from 0.82 GHz to 0.96 GHz, which cannot satisfy the full band requirements in some circumstances.

The reverse situation in which HB elements cause detrimental effects on the LB radiation patterns can also be serious, however, it is seldom discussed in the literature, and has remained as a major challenge to the cellular industry. This situation occurs when the HB elements resonate in the low band, resulting in strong LB currents induced on the HB elements and causing severe distortion of the LB patterns. Although the effect is usually limited to a fairly narrow range of frequencies, it can be detrimental to the system performance.

The **contributions** of the paper are as follows. **1)** For the first time in the literature, the inherent reason of the detrimental effect of HB elements on LB patterns in a dual-band antenna array is analyzed. Clarifying the cause of the challenging but commonly neglected issue would facilitate the development of possible solutions to address it. **2)** To rectify the problem, we propose a feasible solution which is to introduce additional capacitance into the HB antenna structure, realizing a capacitance-loaded HB element. The addition of the series capacitances moves the HB common-mode resonance well outside of the low band of interest, thus successfully restore the LB patterns. **3)** A double-arm choked cross-dipole configuration is innovated as the LB element to enhance the low-frequency operating bandwidth and eliminate the influence of the LB element on HB patterns.

A dual-band array section is constructed with the innovated HB and LB elements to verify the effectiveness of our proposed methods. It covers the low band from 698 MHz to 960 MHz and the high band from 1700 MHz to 2200 MHz. The experimental results demonstrate that the cross-band scattering in the array is largely eliminated, and consistent radiation performance is preserved in both bands. The techniques presented in this article provide effective solutions to the cross-band scattering problem in multi-band antenna arrays in 3G/4G systems, and can also be migrated to 4G/5G systems.

II. THE INFLUENCE OF HB ELEMENTS ON LB RADIATION PERFORMANCE

A typical interleaved dual-band antenna array section as shown in Fig. 1 is used to demonstrate the detrimental effect of HB elements on LB radiation performance. In the array section, the cross-dipole antennas with balun feeds are used as LB and HB elements [8]. The LB element is located midway between the two columns of HB elements. The two HB columns are used separately, and the elements with the same polarization in each column are excited simultaneously using power dividers. The LB element is fed at the inputs to its two baluns.
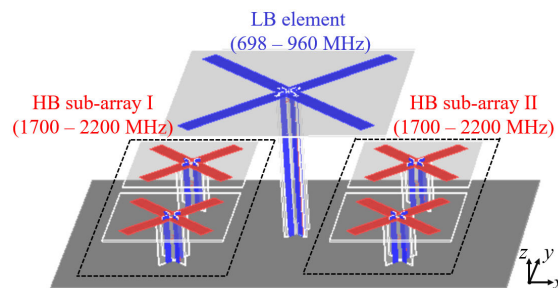

FIGURE 1. Configuration of a dual-band base station antenna array section.
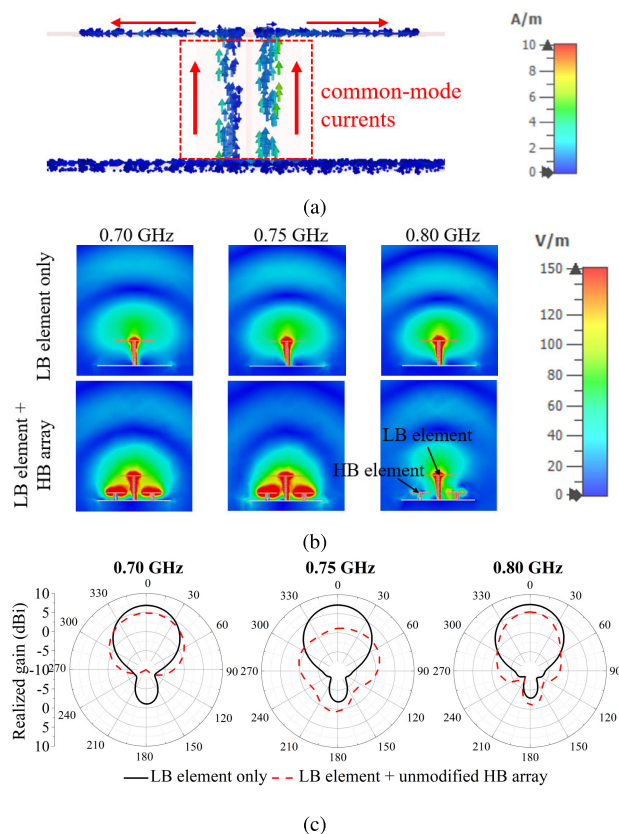

FIGURE 2. (a) The induced LB currents on the HB element at 0.75 GHz. (b) The electric-field distribution, and (c) the horizontal radiation patterns in the low band in the cases of i) only LB element, and ii) LB element with HB array.

When the LB element is excited, there is a significant amount of current induced on the HB elements at around 0.75 GHz, as shown in Fig. 2(a). The currents flowing on the HB radiating arms and parallel lines of the baluns have similar phases and amplitudes, and so are referred to as common-mode currents as distinct from the differential currents that normally feed the dipole. Fig. 2(b) shows the electric-field (E-field) distribution in a horizontal section through the array across the low band in the cases of i) LB element only, and ii) LB element with HB array. It shows that the HB elements are strongly excited at frequencies lower than 0.8 GHz. The excited common-mode currents on the HB elements re-radiate and largely deform the original LB E-field.
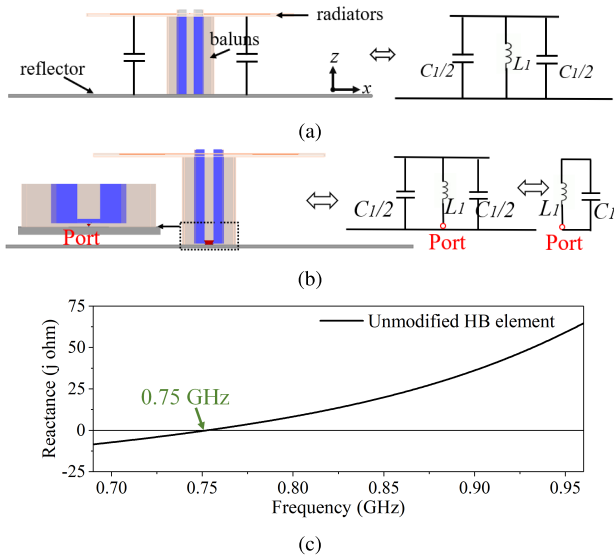
FIGURE 3. (a) Circuit model of the unmodified HB element. (b) Antenna model for finding the resonance of the unmodified HB element. (c) The reactance of the unmodified HB element.

The resultant LB radiation patterns in the horizontal plane (the xz-plane) are shown in Fig. 2(c). The LB patterns without the HB array are also presented for comparison. *It is clear that the LB patterns are greatly distorted in the presence of HB array from 0.698 GHz to 0.80 GHz.* Across this band, the LB patterns are significantly widened and the realized gains are dramatically reduced. The distortion is most severe at around 0.75 GHz where the radiation is no longer directional. The distorted radiation performance is unacceptable for cellular systems.

III. THE CAPACITANCE-LOADED HB ELEMENTS

A. OPERATING MECHANISM OF THE CAPACITANCE-LOADED HB ELEMENT

The induced common-mode currents on HB elements at 0.75 GHz shown in Section II indicate that the HB elements have a common-mode resonance at that frequency. This can be understood using a simplified circuit model shown in Fig. 3(a), where C_1 represents the capacitance between the radiator and the reflector and L_1 represents the inductance of the parallel lines of the baluns and the radiating arms. The resonant frequency of the circuit model is given by

$$f_1 = \frac{1}{2\pi\sqrt{L_1 C_1}} \qquad (1)$$

A model shown in Fig. 3(b) is used in the full-wave simulation to find the resonant frequency f_1. The parallel lines of the baluns are disconnected from the reflector and are joined together. A discrete port is placed between the joined lines and the reflector. By examining the input impedance at the discrete port, the series resonant frequency f_1 is found to be 0.75 GHz as shown in Fig. 3(c).

To minimize the scattering by the HB elements at the low band, it suffices to move the resonant frequency well outside the low band of interest. Here we propose a feasible method to achieve that by series loading another capacitance
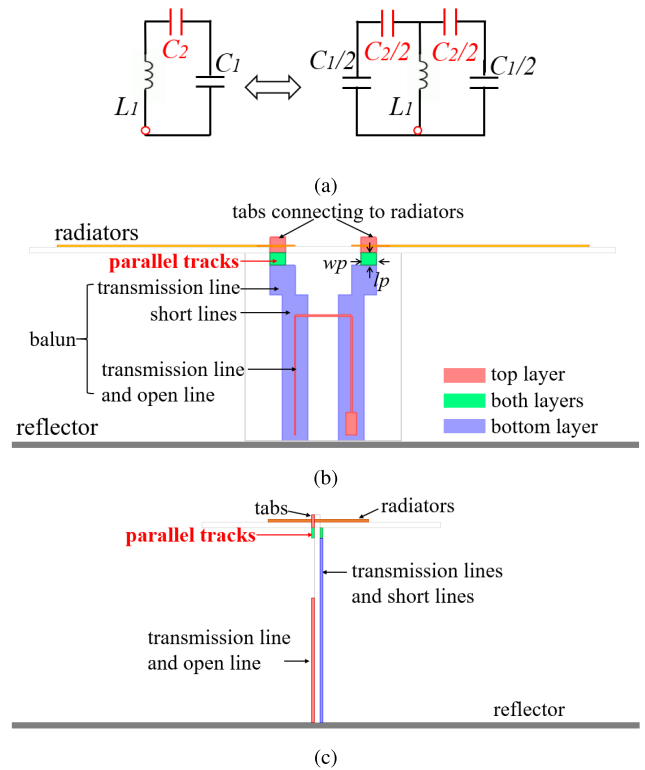

FIGURE 4. (a) Circuit model of the capacitance-loaded HB element. (b) Front view, and (c) side view of the realized capacitance-loaded HB element.

C_2, as shown in Fig. 4(a). With additional C_2, the resonant frequency of the circuit is

$$f_2 = \frac{1}{2\pi}\sqrt{\frac{C_1 + C_2}{C_1 C_2 L_1}} \qquad (2)$$

The ratio between f_2 and the original resonant frequency f_1 is

$$\frac{f_2}{f_1} = \sqrt{\frac{C_1}{C_2} + 1} \qquad (3)$$

It indicates that we can move the resonant frequency by selecting a suitable value of C_2, and a smaller C_2 moves the resonance to a higher frequency. To guarantee minimum influence at the low band, the resonant frequency f_2 should be moved to higher than about 1.05 GHz as found in the simulation.

In the full-wave simulation, the C_2 is realized using small capacitances consisting of parallel tracks on each side of the substrate between the radiators and the balun, as shown in Figs. 4(b) and 4(c). The length and width of the tracks are lp and wp, respectively. A smaller area of $lp \cdot wp$ results in a smaller C_2, thus moving the common-mode resonance f_2 to a higher frequency. However, a smaller C_2 introduces a great capacitive reactance at the high band, which affects the impedance matching of the HB element. Therefore, the value of the capacitance should be carefully adjusted to move the common-mode resonant frequency out of the low band while still allowing the matching of the HB element. The detailed
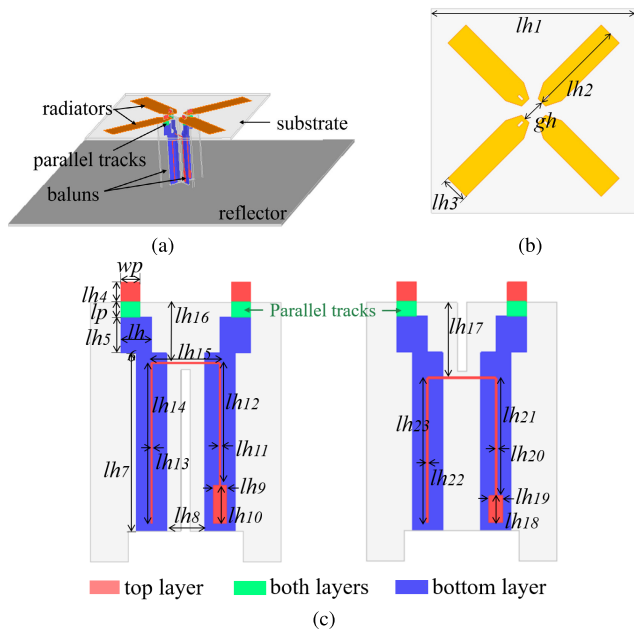
FIGURE 5. Configuration of the HB antenna: (a) perspective view, (b) the radiator, (c) two baluns with added series capacitance.

FIGURE 6. The influence of (a) *lp* and (b) *wp* on moving resonant point f_2.

FIGURE 7. The influence of (a) *lp* and (b) *wp* on the input impedance of HB radiator after series connected with the parallel tracks.

design procedures of the capacitance-loaded HB element are presented as follows.

B. DESIGN OF THE CAPACITANCE-LOADED HB ELEMENT

The complete configuration of the capacitance-loaded HB element is shown in Fig. 5. It includes the cross-dipole radiators, the parallel-track capacitances, the baluns, and the reflector. The design objectives of the capacitance loaded HB element are: 1) moving the common-mode resonant frequency out of low band, so as to reduce the LB currents on the HB element and hence the restoration of LB radiation; and 2) maintaining good impedance matching and radiation performance across the high band. As shown in Figs. 4 and 5, the common-mode resonance is determined by the radiating arms, the capacitors, and the parallel lines of the balun, whereas the differential-mode resonance can be tuned and matched by adjusting the distance between parallel lines (short lines, SL), and the dimensions of the transmission lines (TL) and the open line (OL) in balun. The adjustment carried out to tune and match the differential-mode resonance has little effect on the common-mode resonance. Therefore, the design objectives can be achieved by choosing suitable dimensions of the parallel tracks and adjusting the associated impedance matching network. These will be detailed as follows.

1) DETERMINATION OF THE DIMENSIONS OF THE PARALLEL TRACKS

The added parallel tracks not only affect the moved resonant frequency f_2 at low band, but also influence the input impedance of the element at high band. The moved resonant frequency f_2 with different values of *lp* and *wp* are shown in Fig. 6. A smaller *lp* or *wp* moves f_2 to a higher frequency as it introduces a smaller C_2. The input impedances after adding
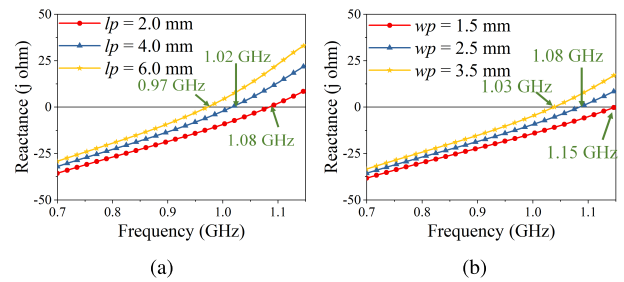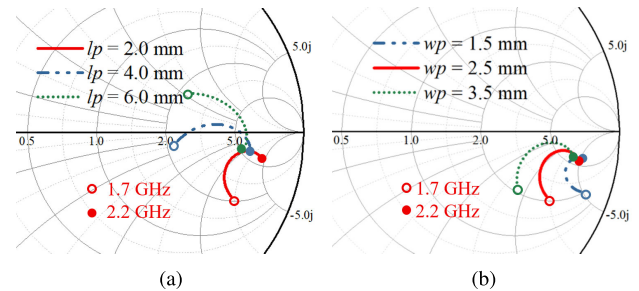
the parallel tracks with different *lp* and *wp* values are shown in Fig. 7. The two parameters have little influence on the input resistance but affect the reactance dramatically. A smaller *lp* or *wp* value introduces a great capacitive reactance, which affects the impedance matching of the HB element. The combination of *wp* = 2.5 mm, *lp* = 2.0 mm with f_2 at 1.08 GHz is selected in the final design of the HB element. It is a compromise between the resultant moved common-mode resonance and the HB impedance match capability.

2) IMPEDANCE MATCHING OF THE HB ELEMENT

After optimizing the parameters for the parallel tracks, the HB radiator is further connected with the baluns to tune the differential-mode resonance and achieve impedance matching. The impedance matching networks included in the balun design follow the guidelines in [9], [10]. Firstly the input impedance of the HB element is matched with the circuit model of balun comprising transmission lines (TL), open line (OL), and short line (SL), as shown in Fig. 8. The parameters for the circuit elements are optimized to achieve the best matching, which are also presented in Fig. 8. Based on the circuit model, the balun is further implemented using microstrip lines shown in Fig. 5(c). The initial parameters of microstrip lines are calculated based on the optimized parameters for circuit elements, and then they are slightly re-adjusted to compensate the discrepancy between the circuit and microstrip models. As a result, both the circuit and microstrip models can match the HB element to reflection coefficients less than −15 dB from 1.67 GHz to 2.18 GHz. All the optimized dimensions of the HB elements are listed in Table 1. All substrates used in this work have a dielectric constant of 4.4, a thickness of 1 mm, and a loss tangent of 0.0025.
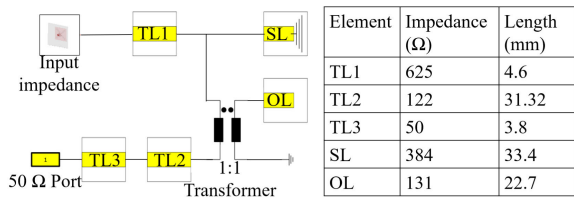
FIGURE 8. Circuit model of the balun, and the optimized parameters for the circuit elements.

TABLE 1. Dimensions of the HB Element (in mm).

Parameter	Value	Parameter	Value	Parameter	Value
gh	9	lp	2	wp	2.5
lh1	80	lh2	38	lh3	10
lh4	2.5	lh5	4.7	lh6	4
lh7	23.3	lh8	5	lh9	1.75
lh10	5	lh11	0.25	lh12	16.125
lh13	0.2	lh14	21.1	lh15	9.225
lh16	7.725	lh17	9.75	lh18	3.5
lh19	1.8	lh20	0.27	lh21	15.62
lh22	0.2	lh23	19.1		

C. PERFORMANCE OF THE CAPACITANCE-LOADED HB ELEMENT

1) MITIGATION OF HB ELEMENT's INFLUENCE ON THE LB RADIATION PERFORMANCE

To verify the effectiveness of the proposed method in restoring the LB radiation performance, the E-field cuts, the horizontal radiation patterns, and the reflection coefficients of the LB element with the capacitance-loaded HB elements are shown in Figs. 9(a), 9(b), and 9(c) respectively. Comparing Fig. 9(a) with Fig. 2(b), we can observe that the modified HB elements have much less influence on the LB E-field than the unmodified HB elements. As a result, the distorted LB patterns by the unmodified HB elements are largely restored by introducing additional capacitances to the HB elements, as shown in Fig. 9(b). The LB patterns and the realized gains with or without the modified HB array are almost identical. Fig. 9(c) shows that the unmodified HB elements also have a destructive effect on the LB reflection coefficient, especially at around 0.75 GHz due to the common-mode resonance of the HB elements, whereas the modified HB elements have little influence on the LB matching result. All the results demonstrate the effectiveness of the capacitance loading technique in moving the common-mode resonance and minimizing the HB antenna's influence on the LB performance.

2) IMPEDANCE MATCHING AND RADIATION PERFORMANCE

The matching result of the capacitance-loaded HB element is shown in Fig. 10(a). The S-parameters of the unmodified HB element (without additional capacitance) is shown in Fig. 10(b) for comparison. Note that these two antennas have different baluns for matching as their input impedance are different. Both antennas are well matched to reflection coefficients less than −15 dB from 1.7 GHz to 2.17 GHz. The HB horizontal radiation patterns of the HB antennas with and without capacitance loading are presented in Figs. 10(c) and 10(d). The inclusion of C_2 has a negligible effect on the HB patterns which are stable across the operating band.
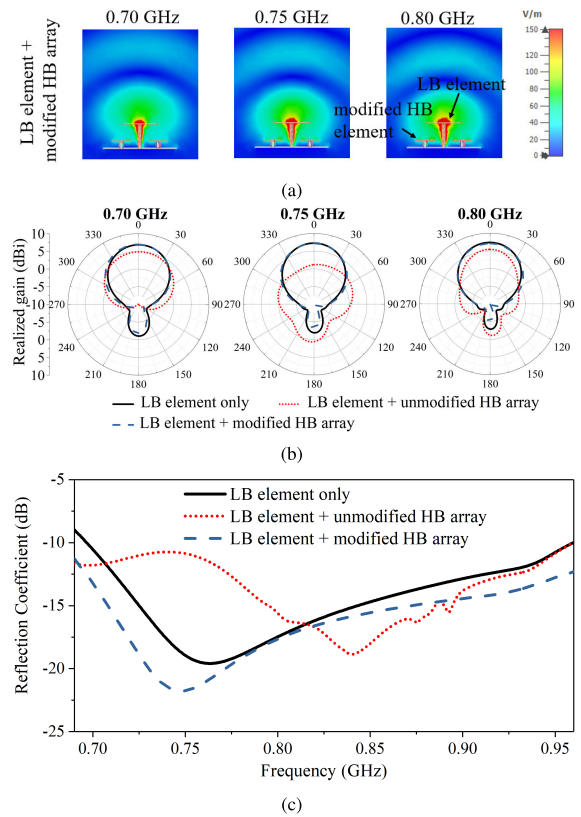

FIGURE 9. (a) The electric-field distribution of the LB element with the capacitance-loaded HB array. The comparison of (b) the LB radiation patterns, and (c) the LB reflection coefficients in three cases: i) LB element only, ii) LB element with unmodified HB array (without capacitance loading), and iii) LB element with the capacitance-loaded HB array.
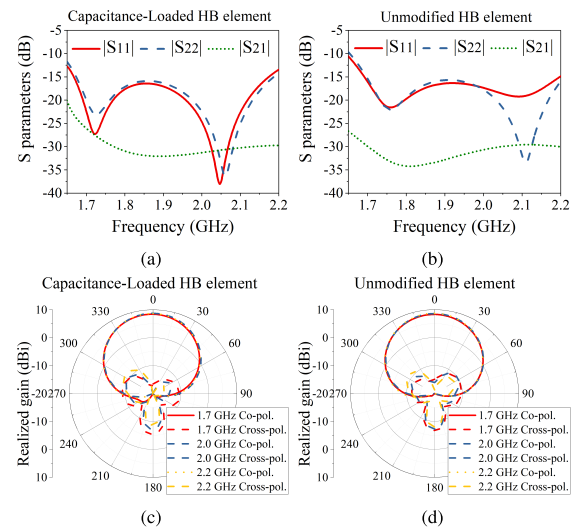

FIGURE 10. Comparison of S-parameters for (a) the capacitance-loaded HB element, and (b) the original HB element without capacitance loading. Comparison of radiation patterns for (c) the capacitance-loaded HB element and (d) the original HB element without capacitance loading.

These results show that the addition of the capacitance to the HB element does not degrade the original HB performance.

IV. WIDEBAND DOUBLE-ARM CHOKED LB ELEMENT

The choking method has been used to suppress HB scattering caused by the LB element. However, the chokes introduce
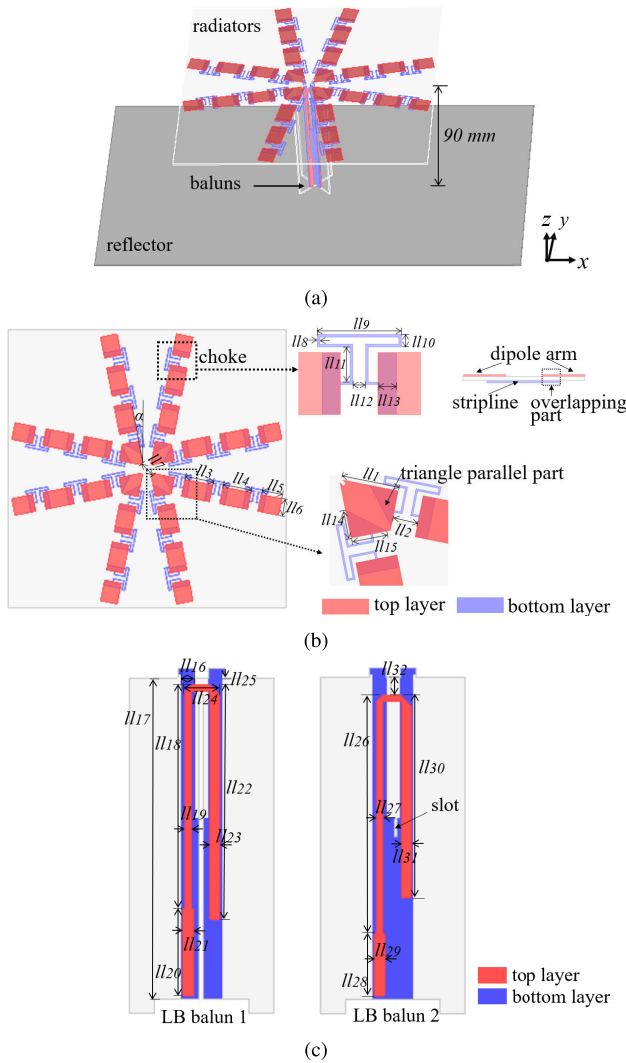
FIGURE 11. Configuration of the double-arm choked LB element: (a) perspective view of the LB element, (b) the view of the radiator, and (c) the views of baluns.

FIGURE 12. (a) The configurations of the single-arm cross-dipole, the double-arm sub-dipole, and the double-arm cross-dipole radiators. (b) Input impedances of the three radiators on the Smith chart from 0.698 GHz to 0.96 GHz.

TABLE 2. Dimensions of the LB Element (in mm).

Parameter	Value	Parameter	Value	Parameter	Value
ll1	14.8	*ll2*	6.7	*ll3*	18.5
ll4	18.5	*ll5*	13.7	*ll6*	11
ll7	11	*ll8*	0.47	*ll9*	15
ll10	2.22	*ll11*	6.265	*ll12*	2.3
ll13	3.25	*ll14*	7.53	*ll15*	9.5
ll16	3.5	*ll17*	89	*ll18*	61.85
ll19	1.7	*ll20*	24	*ll21*	3.25
ll22	64.85	*ll23*	2.7	*ll24*	9.7
ll25	2	*ll26*	65.85	*ll27*	1.7
ll28	17	*ll29*	2.8	*ll30*	55.85
ll31	2.9	*ll32*	5	α	11°

a large variation in the input impedance of the radiators and narrow the operating bandwidth of the LB element [1]. As analyzed in [11], [12], the bandwidth of a cross-dipole antenna can be broadened by introducing mutual coupling between the two orthogonally oriented sub-dipoles. This is usually achieved by widening the dipole arms [8], [13], and modifying the shape of the arms [14], [15] to bring the sub-dipoles close to each other. However, wide dipole arms and complex arm shapes are difficult to integrate with chokes. In this work, we propose a double-arm structure to have the chokes inserted in and to take advantage of the coupling between adjacent radiating arms thereby enhancing the bandwidth.

The complete configuration of the double-arm choked LB element is shown in Fig. 11. As shown in Fig. 11(b), each dipole arm is composed of two obliquely positioned strips connected at a common feeding point. Three chokes are inserted into each strip to effectively divide the strip into short pieces that are well below resonance in the high band.
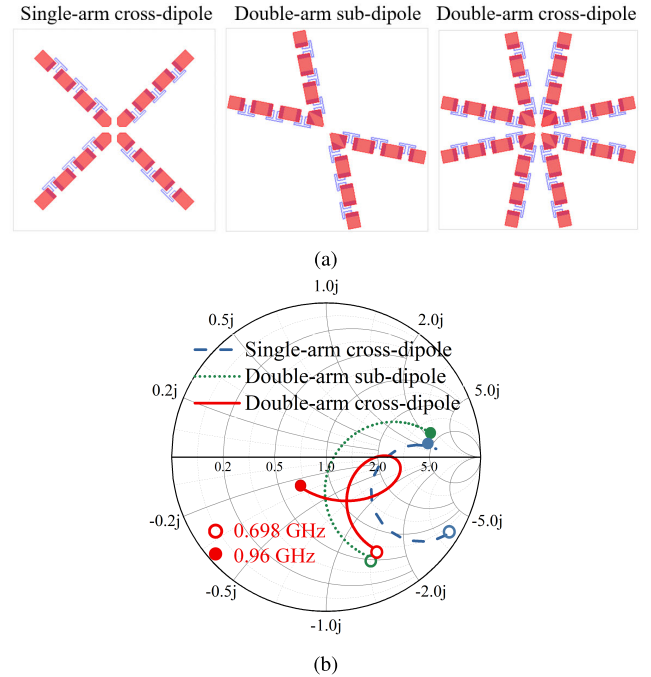
This ensures that HB currents induced on them are greatly reduced compared with the original configuration. The chokes have an open-circuit resonance at 1.78 GHz as this was found to minimize the maximum HB induced current on LB arms. The chokes are designed with a Ω shape to reduce the occupied area and avoid crossovers with other chokes in adjacent arms. The parallel plate capacitances in the chokes near the feed point of dipoles are modified with a triangular shape to avoid overlapping with adjacent chokes.

To demonstrate how the double-arm cross-dipole configuration facilitates the impedance matching, the input impedances of three radiators are analyzed, as shown in Fig. 12. The radiators are a single-arm choked cross-dipole, a double-arm choked sub-dipole, and a double-arm cross-dipole. All the radiators are placed above a reflector at a distance of 90 mm. The input impedances of the radiators from 0.698 GHz to 0.96 GHz on the Smith Chart are presented in Fig. 12(b). Both the resistance and reactance of the single-arm cross-dipole fluctuate greatly, making it knotty
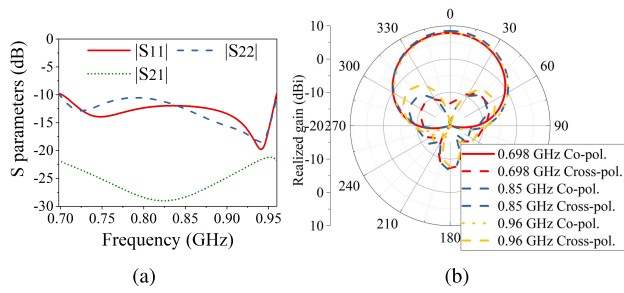
FIGURE 13. (a) S-parameters, and (b) horizontal radiation patterns of the double-arm choked LB element.
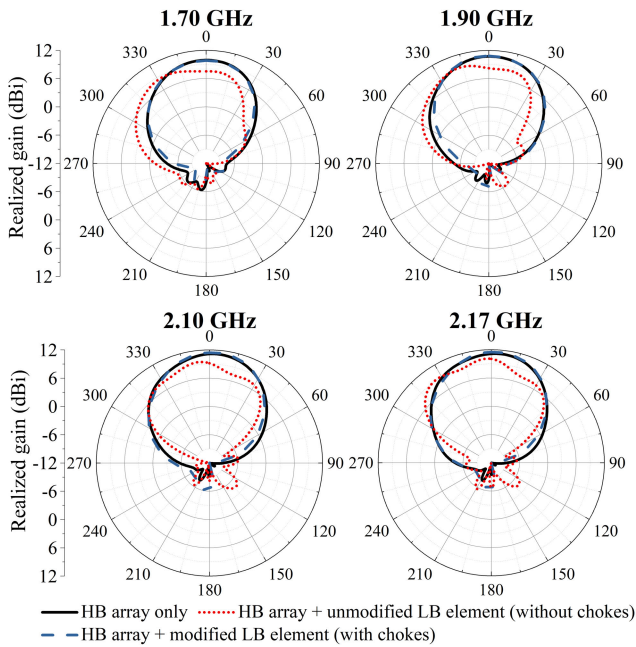

FIGURE 14. Comparison of horizontal HB radiation patterns under the circumstances of i) HB array only, ii) HB array with unmodified LB element (without chokes), and iii) HB array with the double-arm choked LB element.

for the radiator to be matched well across the targeted band. The variation in input impedance of double-arm sub-dipole is still significant. However, with the addition of the other sub-dipole, the fluctuations in input impedance of the double-arm cross-dipole are greatly alleviated. The introduced coupling with the proposed double-arm structure results in a typical double-tuned trace, which makes the matching significantly simpler.

The double-arm cross-dipole radiator is further matched with baluns, as shown in Fig. 11(c). A small slot is cut in balun 2 to insert a shorting patch that connects the parallel lines of balun 1. All the parameters of the choked LB element are listed in Table 2. The matching result is presented in Fig. 13(a). The LB element is matched from 0.698 GHz to 0.96 GHz with reflection coefficients less than −10 dB. Compared with [1], the bandwidth is improved by 11%, and it fully covers the LTE 700MHz/ GSM 850MHz/ GSM 900MHz bands as required by the cellular industry. The horizontal radiation patterns of the LB element with a $400 \times 400 \text{ mm}^2$ square reflector are presented in Fig. 13(b). The radiation performance is consistent across the operating band.

The performance of the double-arm choked LB element in eliminating the HB scattering is examined in dual-band arrays. The radiation patterns of the HB array with or without the proposed LB element are shown in Fig. 14. The HB patterns in the presence of the unmodified LB element (without chokes) are also added for comparison. It is clear that the existence of the unmodified LB element causes the distortion of HB radiation patterns and leads to gain loss, whereas the proposed choked LB element effectively restores the original HB patterns with little influence on the gain. The comparison shows the effectiveness of the innovated choked LB element in reducing the HB pattern distortion. All the results in this section demonstrate that the proposed double-arm choked cross-dipole structure as an LB element can broaden the low-frequency bandwidth and effectively suppress the HB scattering.

V. THE PERFORMANCE OF THE DUAL-BAND ARRAY SECTION

A dual-band array section is built according to the techniques described above, as shown in Fig. 15. The HB sub-arrays are fed by power dividers, where the HB elements with the same polarization in one sub-array are excited simultaneously. The LB element is fed by coaxial cables directly connected to the LB balun. Ports 1 − 4 are HB ports, and Ports 5 and 6 are LB ports. Fig. 15(c) shows the array section as built and tested. Coaxial cables are used to connect HB feed points with power dividers.
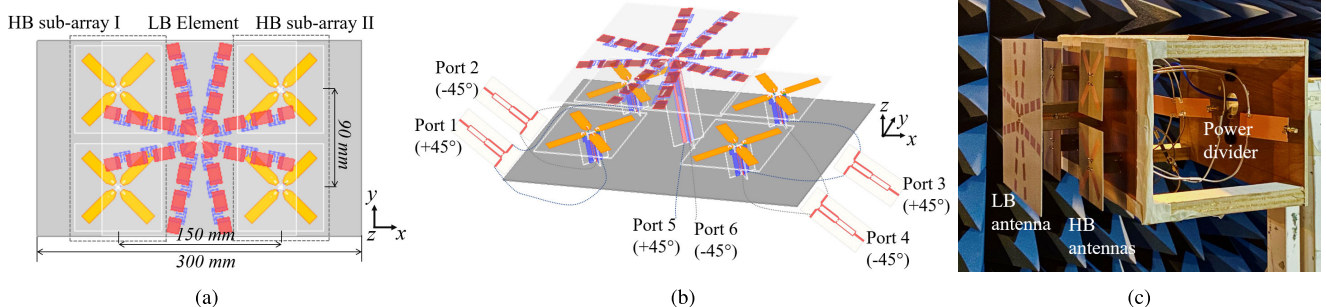

FIGURE 15. (a) Top view, and (b) perspective view of the dual-band array section. (c) Perspective view of the fabricated prototype.
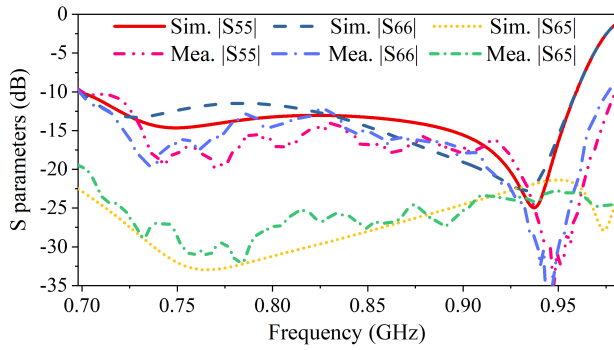
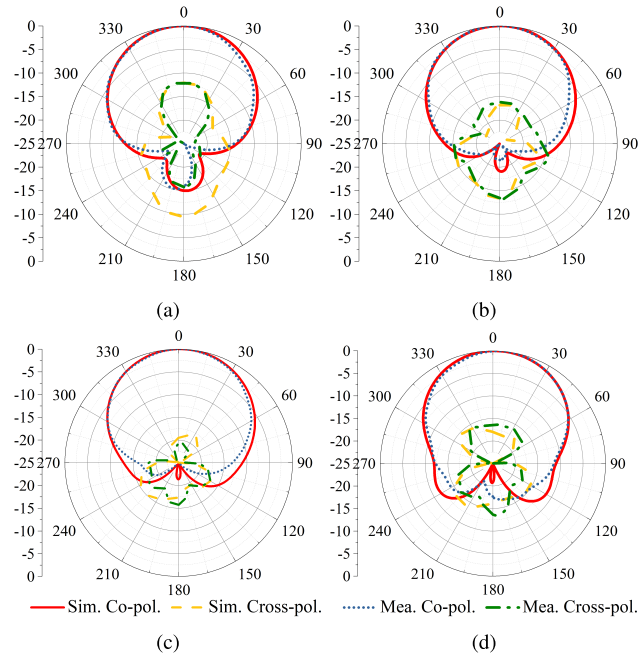**FIGURE 16.** Simulated and measured S-parameters of the LB antenna.

FIGURE 17. Normalized radiation patterns in the horizontal plane of the +45° radiation of the LB element at (a) 0.7 GHz, (b) 0.8 GHz, (c) 0.9 GHz, (d) 0.96 GHz.
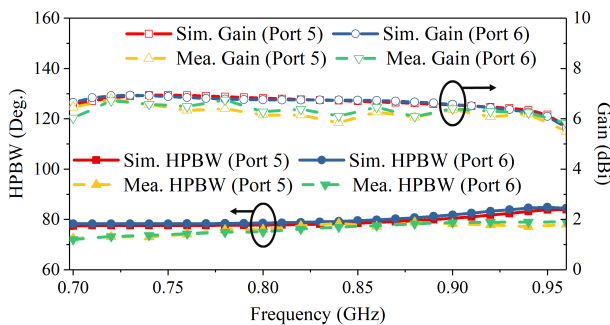

FIGURE 18. Simulated and measured HPBW and gain of the LB antenna.

The experimental results of the LB element are presented in Figs. 16 - 18. Fig. 16 shows the LB element has a measured bandwidth of 33.6% from 0.698 GHz to 0.98 GHz for reflection coefficients less than −10 dB. It is slightly wider than the simulated results, which can be caused by the loss of cables and substrates. Across the band, the measured port isolation
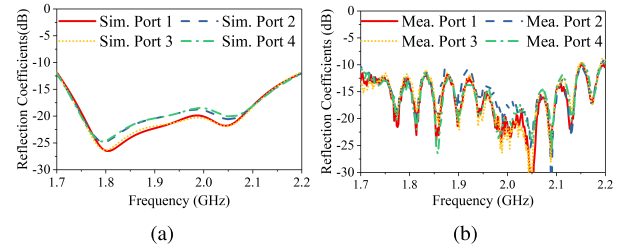

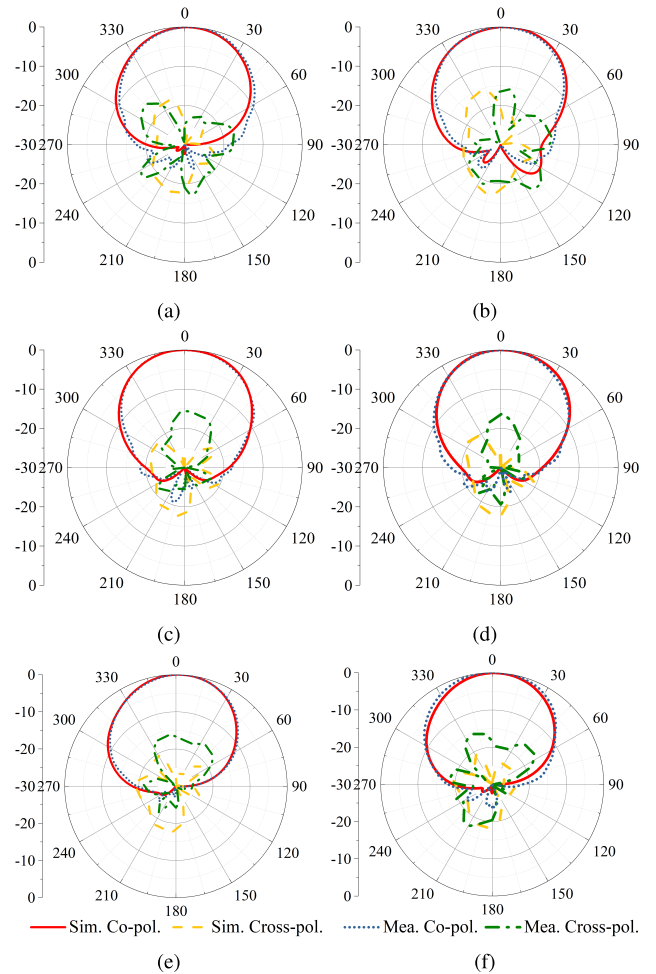**FIGURE 19.** (a) Simulated and (b) measured reflection coefficients of HB ports.

FIGURE 20. Normalized radiation patterns in the horizontal plane of the HB sub-array. (a) Port 1 at 1.7 GHz, (b) port 2 at 1.7 GHz, (c) port 1 at 1.9 GHz, (d) port 2 at 1.9 GHz, (e) port 1 at 2.1 GHz, and (f) port 2 at 2.1 GHz.

is above 20 dB. Fig. 17 shows the simulated and measured horizontal radiation patterns of the −45° polarization at 0.7 GHz, 0.8 GHz, 0.9 GHz, and 0.96 GHz. The patterns of the +45° polarization are similar due to the symmetry of the structure. The simulated and measured patterns are almost identical. The cross-polarization levels are less than −13 dB at boresight and less than −9 dB within ±60° coverage. The horizontal half-power beamwidth (HPBW) and gain of the LB element are presented in Fig. 18. The measured radiation patterns are stable with horizontal HPBW of 75°±5°.
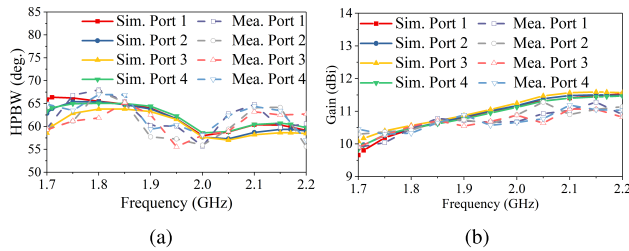
FIGURE 21. Simulated and measured (a) HPBW and (b) gain of the HB sub-arrays.

The gain varies from 5.5 dBi to 6.8 dBi across the band. The slightly low gain is caused by the small size of the reflector in the demonstrated array section. It can be improved with a larger reflector. The simulated total efficiency of the LB antenna is above 80% across the band.

Fig. 19 - 21 shows the performance of the HB sub-arrays. Fig. 19 shows the HB sub-arrays operate from 1.7 GHz to 2.2 GHz with reflection coefficients less than −10 dB. The discrepancy between the simulated and measured results, especially the large ripples in the measured curves, can be caused by the multiple reflections of the antennas, cables, power dividers, and their connecting points. The HB radiation patterns of the two polarizations in one of the HB sub-arrays are plotted in Fig. 20. The measured patterns are in good agreement with the simulated ones. The cross-polarization levels are less than −15 dB at the boresight. Figs. 21(a) and 21(b) show the horizontal HPBW and realized gain of the HB sub-arrays, respectively. The radiation patterns are stable with measured HPBWs of 64°±5°. The simulated and measured gain are 10.6±1.0 dBi and 10.5±0.5 dBi, respectively. The small discrepancy can be caused by the fabrication and measurement tolerance. The simulated total efficiency of the HB sub-arrays is above 85% across the operating band.

The experiment results of the array section show consistent radiation performance across the well-matched low and high bands, demonstrating the effectiveness of the presented techniques in suppressing the cross-band mutual scattering and enhancing the low-frequency bandwidth.

VI. CONCLUSION

In this article, we first analyze the LB scattering issue caused by the common-mode resonance of the HB elements in dual-band antenna arrays. To mitigate the detrimental effect of HB elements on LB patterns, a capacitance loading technique is proposed and applied to the HB element to move the common-mode resonance outside of the low band of interest. Secondly, we innovate a double-arm choked LB element to suppress the HB scattering and enhance the low-frequency bandwidth. An array section is constructed with the innovated LB and HB elements to verify their performance. The experimental results of the array show reduced cross-band pattern degradation and stable radiation performance across the low and high bands. The techniques presented in the work serve as solutions to suppress the cross-band scattering in multi-band antenna arrays, which help to facilitate the evolution of advanced antenna systems.

REFERENCES

[1] H.-H. Sun, C. Ding, H. Zhu, B. Jones, and Y. J. Guo, "Suppression of cross-band scattering in multiband antenna arrays," *IEEE Trans. Antennas Propag.*, vol. 67, no. 4, pp. 2379–2389, Apr. 2019.

[2] H. Huang, Y. Liu, and S. Gong, "A novel dual-broadband and dual-polarized antenna for 2G/3G/LTE base stations," *IEEE Trans. Antennas Propag.*, vol. 64, no. 9, pp. 4113–4118, Sep. 2016.

[3] H. Huang, Y. Liu, and S. Gong, "A dual-broadband, dual-polarized base station antenna for 2G/3G/4G applications," *IEEE Antennas Wireless Propag. Lett.*, vol. 16, pp. 1111–1114, 2017.

[4] Y. He, Z. Pan, X. Cheng, Y. He, J. Qiao, and M. M. Tentzeris, "A novel dual-band, dual-polarized, miniaturized and low-profile base station antenna," *IEEE Trans. Antennas Propag.*, vol. 63, no. 12, pp. 5399–5408, Dec. 2015.

[5] M. Kaboli, M. S. Abrishamian, S. A. Mirtaheri, and S. M. Aboutorab, "High-isolation XX-polar antenna," *IEEE Trans. Antennas Propag.*, vol. 60, no. 9, pp. 4046–4055, Sep. 2012.

[6] Y. Zhu, Y. Chen, and S. Yang, "Decoupling and low-profile design of dual-band dual-polarized base station antennas using frequency-selective surface," *IEEE Trans. Antennas Propag.*, vol. 67, no. 8, pp. 5272–5281, Aug. 2019.

[7] Y. Chen, J. Zhao, and S. Yang, "A novel stacked antenna configuration and its applications in dual-band shared-aperture base station antenna array designs," *IEEE Trans. Antennas Propag.*, vol. 67, no. 12, pp. 7234–7241, Dec. 2019.

[8] Y. Cui, R. Li, and H. Fu, "A broadband dual-polarized planar antenna for 2G/3G/LTE base stations," *IEEE Trans. Antennas Propag.*, vol. 62, no. 9, pp. 4836–4840, Sep. 2014.

[9] W. Roberts, "A new wide-band balun," *Proc. IRE*, vol. 45, no. 12, pp. 1628–1631, 1957.

[10] H. Sun, C. Ding, B. Jones, and Y. J. Guo, "A wideband base station antenna element with stable radiation pattern and reduced beam squint," *IEEE Access*, vol. 5, pp. 23022–23031, Oct. 2017.

[11] Z. Bao, Z. Nie, and X. Zong, "A novel broadband dual-polarization antenna utilizing strong mutual coupling," *IEEE Trans. Antennas Propag.*, vol. 62, no. 1, pp. 450–454, Jan. 2014.

[12] C. Ding, H. Sun, R. W. Ziolkowski, and Y. J. Guo, "Simplified tightly-coupled cross-dipole arrangement for base station applications," *IEEE Access*, vol. 5, pp. 27491–27503, Nov. 2017.

[13] Y. Gou, S. Yang, J. Li, and Z. Nie, "A compact dual-polarized printed dipole antenna with high isolation for wideband base station applications," *IEEE Trans. Antennas Propag.*, vol. 62, no. 8, pp. 4392–4395, Aug. 2014.

[14] H.-H. Sun, C. Ding, H. Zhu, and Y. J. Guo, "Dual-polarized multi-resonance antennas with broad bandwidths and compact sizes for base station applications," *IEEE Open J. Antennas Propag.*, vol. 1, pp. 11–19, Jan. 2020.

[15] H. Huang, Y. Liu, and S. Gong, "A broadband dual-polarized base station antenna with sturdy construction," *IEEE Antennas Wireless Propag. Lett.*, vol. 16, pp. 665–668, Mar. 2017.

HAI-HAN SUN (Member, IEEE) received the bachelor's degree in electronic information engineering from the Beijing University of Posts and Telecommunications, Beijing, China, in 2015, and the Ph.D. degree in engineering from the University of Technology Sydney, Australia, in 2019. She is currently a Research Fellow with the School of Electrical and Electronic Engineering, Nanyang Technological University, Singapore. Her research interests include base station antennas and ground penetrating radar.

BEVAN JONES was born in Sydney, Australia. He received the B.Sc. degree, the B.E. degree (Hons.), and the Ph.D. degree in electrical engineering from the University of Sydney, Australia, in 1967, 1970, and 1974, respectively.

From 1974 to 1977, he was a Postdoctoral Fellow with the Max-Planck-Institut für Radioastronomie, Bonn, Germany on the design of a millimeter wavelength radio-telescope. After two years as a Lecturer at Wollongong University, Australia, he returned to Germany as a Scientist to continue his previous work. In 1980, he returned to Australia, to work on the Interscan Project to develop a microwave aircraft landing system (MLS). From 1980 to 1982, he led a group of 12 Australian engineers working on this project in the USA with a joint venture partner. From 1983 to 1994, he was the Technical Director of Interscan Australia Pty Ltd., an R&D company owned and funded by the Australian Industry Development Corporation (AIDC). He led the development of many antenna based products including the microwave landing system (MLS), a C-band phased array precision approach systems, an electronically scanned TACAN navigation beacon, a large vertical aperture secondary surveillance radar antenna and an advanced S-band multi-beam phased array primary radar antenna. He was also responsible in 1992–1993 for the development of early cellular base station antennas, the first with adjustable electrical beam tilt at the time when the original AMPS system was being rolled out. In 1994, together with two partners, he founded Argus Technologies, Australia, and served as the Managing Director for ten years and then as the Technical Director. The company has specialized solely in the design and manufacture of cellular base station antennas and expanded its market reach worldwide. The company initially operated in Sydney but set up a second manufacturing facility in Guangzhou, China, in 2001, and later established an R&D capability there. Since its inception, Argus has brought many innovations to market and became a major international supplier of cellular antennas. In 2011, the company was acquired by a U.S. multinational, where he served as the Technical Director under the new ownership for a further two years, during which time he was largely engaged in technical instruction of the group's engineering teams in the U.S. and China. Following that, he retired from full-time work and since then has done a number of consulting jobs on antenna related topics. He is currently an Adjunct Professor with the University of Technology Sydney (UTS). He has authored a number of articles in technical journals and patents relating to antenna components and has done consulting on antennas and electromagnetics for a number of companies, including Raytheon and British Aerospace. He has taught specialist courses in numerical methods and electromagnetics at universities.

Y. JAY GUO (Fellow, IEEE) received the bachelor's and master's degrees from Xidian University, China, in 1982 and 1984, respectively, and the Ph.D. degree from Xi'an Jiaotong University, China, in 1987. He held various senior technology leadership positions in Fujitsu, Siemens, and NEC, U.K. In 2014, he served as the Director for CSIRO for more than 9 years. He is currently a Distinguished Professor and the Director of Global Big Data Technologies Centre (GBDTC), University of Technology Sydney (UTS), Australia. He has published more than 550 research articles, including 280 journal articles, most of which are in IEEE Transactions. He holds 26 patents. His research interests include antennas, mm-wave, and THz communications and sensing systems, and big data technologies.

Dr. Guo is a Fellow of the Australian Academy of Engineering and Technology, a Fellow of IET, and was a member of the College of Experts of Australian Research Council (ARC), from 2016 to 2018. He was a recipient of a number of most prestigious Australian Engineering Excellence Awards, in 2007 and 2012, and the CSIRO Chairman's Medal, in 2007 and 2012. He was named one of the most influential engineers in Australia, in 2014 and 2015, respectively, and one of the top researchers in Australia, in 2020. He has chaired numerous international conferences and served as a guest editor for a number of IEEE publications. He is the Chair of the International Steering Committee and the International Symposium on Antennas and Propagation (ISAP). He was the International Advisory Committee Chair of IEEE VTC2017, a General Chair of ISAP2022, ISAP2015, iWAT2014, and WPMC'2014, and a TPC Chair of 2010 IEEE WCNC, and 2012 and 2007 IEEE ISCIT. He served as a Guest Editor for Special Issues on "Antennas for Satellite Communications" and "Antennas and Propagation Aspects of 60-90GHz Wireless Communications," both in the IEEE Transactions on Antennas and Propagation, Special Issue on "Communications Challenges and Dynamics for Unmanned Autonomous Vehicles," the IEEE Journal on Selected Areas in Communications (JSAC), and Special Issue on "5G for Mission Critical Machine Communications", the *IEEE Network Magazine*.

YEE HUI LEE (Senior Member, IEEE) received the B.Eng. (Hons.) and M.Eng. degrees from the School of Electrical and Electronics Engineering, Nanyang Technological University, Singapore, in 1996 and 1998, respectively, and the Ph.D. degree from the University of York, York, U.K., in 2002. Since 2002, she has been a Faculty Member with Nanyang Technological University, where she is currently an Associate Professor with the School of Electrical and Electronic Engineering.

Her research interests include channel characterization, rain propagation, remote sensing and radar systems, antenna design, electromagnetic bandgap structures, and evolutionary techniques.

• • •